 doi:10.20944/preprints202207.0060.v1

Article

Design of Broadband Perfect Solar Absorber Based on Four-Layer Structure with Cross-Shaped Resonator and Triangular Array

Yu-Shan Chen[1], Ke-Wei You[1], Wen-Zhaung Ma[1], Dan Meng[1] , Yu-Yao Cheng[1] and Jing Liu *

[1]School of Information Engineering, Jimei University, Xiamen 361021, China
* Correspondence: Correspondence: jingliu@jmu.edu.cn

Abstract: As solar energy is a low-cost and clean energy source, there has been a great deal of interest in how to harvest it. To absorb solar energy efficiently, we have designed a broadband metamaterial absorber based on the principle of Fabry–Pérot (FP) cavity and surface plasmon resonances (SPRs). We propose a broadband perfect absorber consisting of a four-layer structure of silica-tungsten-silica-titanium (SiO_2-W-SiO_2-Ti) for the incident light wavelength range of 300–2500 nm. The structure achieves perfect absorption of incident light in the wavelength range of 351.8–2465.0 nm (absorption >90%), with an average absorption of 96.3%. The advantage of our proposed structure is that it combines the characteristics of both high and broadband absorption and has a high overall absorption efficiency for solar radiation. It is also independent of polarization and insensitive to incident angle. We investigated how absorption was affected by different structures, materials, geometrical parameters, and refractive indices for different dielectric materials, and we explored the reasons for high absorption. This structure is refractory and ultra-thin, and it offers a good trade-off between bandwidth and absorption. It therefore has premium application prospects and value.

Keywords: perfect absorber; ultra-broadband; visible region; near infrared region

1. Introduction

As the global demand for energy has increased dramatically, burning of fossil fuels has led to many environmental problems, such as the greenhouse effect. To minimize the serious consequences of global warming and keep the planet's average surface temperature from rising more than 2°C, the current direction of sustainable development is toward significantly increasing the share of renewable energy in the global energy structure and doubling energy efficiency[1]. Solar energy is a premium and cheap renewable energy source. Many studies have been carried out on the acquisition, storage, and use of solar energy[2-6], especially how to collect it.

Based on a survey of the last decade's literature, we found that metamaterials have many extraordinary properties, because the materials are human selected and their parameters are artificially designed. Metamaterials thus offer a wide range of application scenarios for achieving various purposes through different designs — for example, thermal energy emission[7, 8], photodetection[9, 10], thermoelectric conversion[11, 12], and sensing[13, 14]. In addition, metamaterial absorbers can be very effective for solar harvesting[15, 16].

Because noble metals can provide strong plasmonic resonance and optical coupling, many studies have used them as solar absorbers[17-19]. However, the intrinsic absorption of noble metals means the overall bandwidth of such absorbers is narrow. Li et al. proposed an 11-layer absorber whose optical properties could be tailored by manually changing the parameters of a periodic Au array, but its absorption bandwidth was relatively narrow (400–700 nm)[17]. Also using gold, Qin et al. designed an absorber with three absorption peaks to achieve broadband absorption in the 1000–2500 nm band. However, the absorber had insufficient absorption in the visible light range, and the average absorption rate was less than 70%[18]. Ali Elrashidi and colleagues designed a three-layer absorber composed of Ti, SiO_2, and Ag after trying a variety of materials. This structure realized broadband absorption of 1410 nm[19].

Because the intrinsic absorption of noble metals makes it difficult to achieve broadband absorption, and because of their scarcity, high cost, and poor chemical and physical stability, researchers are paying less attention to precious metals and turning to other types of materials, such as refractory metals. Liu et al. designed a titanium nitride (TiN) nano-resonator array and coated it on a titania (TiO_2) array; together, these provided multiple resonant modes for the entire structure. After a series of parameter adjustments, an absorption bandwidth of 1110 nm was obtained[20]. Yu et al. designed a solar absorber with high thermal stability using a refractory metal. The intrinsic absorption performance and plasmonic resonance of titanium provided 1264 nm broadband absorption[21].

 doi:10.20944/preprints202207.0060.v1

Using silicon nitride as a dielectric material, Liu and other researchers piled four different sized layers of iron, from large to small, obtaining four absorption peaks and achieving 1.4–11.4 μm absorption (>60%). Although the bandwidth of this structure was large, the average absorption rate was low[22]. Wu et al. used Ti and SiO_2 materials with good thermal stability and achieved broadband absorption from 0.596 to 4.102 μm. However, the structure had poor absorption performance for incident light in the visible region, especially in the 500–750 nm wavelength range [23]. The aforementioned absorbers had either high absorption or broadband absorption, but not both. We believe that the most effective absorption of sunlight can only be achieved if both broadband and high absorption can be achieved. In designing our absorber, we avoided noble metals and chose tungsten and titanium, two metals with excellent overall performance.

We propose an ultra-wideband perfect absorber for solar light based on the finite-difference time-domain (FDTD) method. Previous researchers have demonstrated that actual experimental results are highly identical to those obtained using the FDTD method[24, 25]. Therefore, it was feasible to probe the absorption efficiency of our proposed structure with this method. The whole structure is centrosymmetric and axisymmetric, making it independent of polarization as well as insensitive to the incident angle. The attenuation properties of tungsten and titanium mean they have a high imaginary refractive index. Combining the two metals achieved high absorption and broadband absorption at the same time. Both materials also have high melting points, contributing to the structure's overall thermal stability. We can use electron beams to deposit the substrate of this absorber and employ lithography and different etching processes to build cross-shaped resonators and triangular arrays. The structure can be prepared on a large scale due to the absence of noble metal materials. In general, our proposed absorber has the advantages of simple structure, easy preparation, good absorption performance, and thinness, so it holds promise for applications.

2. Model and parameter design of perfect solar absorber

We took full advantage of the absorber's high absorption principle to improve the absorption efficiency and bandwidth. The cross structure of tungsten and the four surrounding tungsten triangular cylinders easily provided powerful surface plasmon resonance. The two layers below (SiO_2 and Ti) cooperated with tungsten to form a FP cavity, which further enhanced the absorption of incident light in the visible to near-infrared bands. In addition, we attached a layer of SiO_2 to the tungsten array to enhance the plasmon resonance, which augmented the absorption of incident light. The refractive index values for tungsten and titanium were obtained from the *CRC Handbook of Chemistry and Physics*[26], and the refractive index of SiO_2 was set at 1.45[27]. We used FDTD Solutions to verify our proposed structure. Periodic conditions were set in the X and Y directions, and PML boundary conditions were set in the Z direction. The optimized material parameters were l = 410 nm, w = 90 nm, t = 150 nm, P = 700 nm, h_1 = 80 nm,

Preprints (www.preprints.org) | NOT PEER-REVIEWED | Posted: 5 July 2022 doi:10.20944/preprints202207.0060.v1

h_2 = 200 nm, h_3 = 60 nm, h_4 = 200 nm. A schematic diagram of the structure, as well as a top view and side view, are shown in Fig. 1.

Fig. 1. (a) Schematic diagram of the periodic structure. (b) Top view of the absorber with its parameters, where l = 410 nm, w = 90 nm, t = 150 nm. (c) Side view of the absorber with its parameters, where P = 700 nm, h_1 = 80 nm, h_3 = 60 nm, h_2 = h_4 = 200 nm.

3. Results and discussion

The formula used to calculate the absorption of the absorbing structure is $A = 1 - R - T$. We set the thickness of the titanium substrate to 200 nm, which resulted in almost no electromagnetic waves penetrating the entire structure, so $T = 0$, therefore $A = 1 - R$. We thus calculated the absorption of the structure for incident light in the wavelength range of 300–2500 nm. As shown in Figure 2a, the absorption curve of this structure possessed three absorption peaks, located at 800, 1320, and 2120 nm, respectively. The

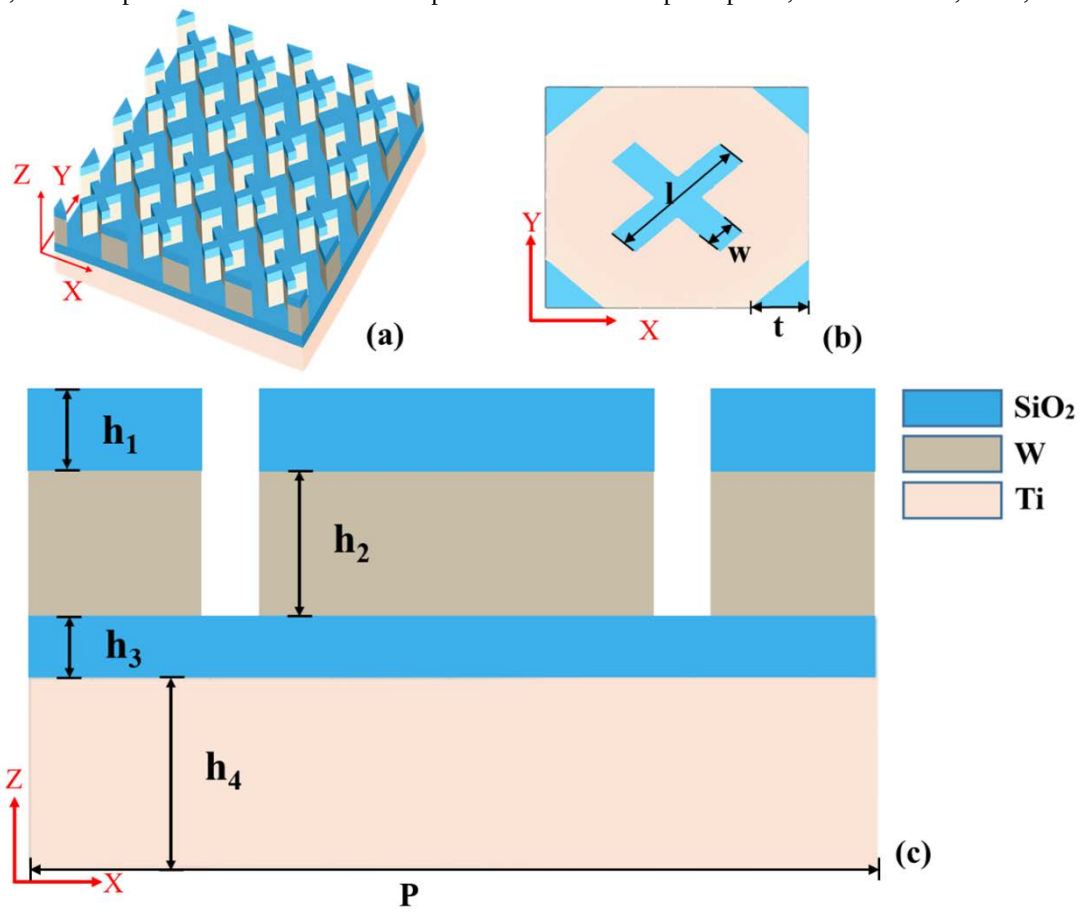

highest absorption value was located at the incident light wavelength of 1320 nm, with a maximum absorption of 99.4%. The perfect absorption region of this structure (absorption >90%) covered almost the entire visible to near-infrared band, with a perfect absorption band width of 2113.2 nm (from 351.8 to 2465.0 nm). Within this perfect absorption band, we calculated the average absorption using the following formula, where λ_2 = 351.8 nm and λ_1 = 2465.0 nm:

$$A = \int_{\lambda_2}^{\lambda_1} A(\lambda) d\lambda / (\lambda_1 - \lambda_2) \quad (1)$$

We used the calculated average absorption to determine the energy absorption of this structure for solar scattering. The results are shown in Fig. 2(b). The proposed structure had only a small energy loss in the visible and ultraviolet (UV) band and absorbed almost all the sunlight in the other bands, indicating its good absorption performance.

We also explored how the absorptivity was affected by a planar structure, the absence of a top dielectric structure, and the use of different materials. The structure with a SiO_2 top layer had a smoother absorption curve than one without, meaning the SiO_2 top layer brought better solar coupling to the whole structure. As shown in Figure 2(c), the structure with a SiO_2 top layer had higher absorption efficiency in the visible wavelength band. The presence of a SiO_2 dielectric made it easier for electromagnetic waves with smaller wavelength values to be absorbed by the whole structure. Within the solar radiation spectrum, the visible band accounts for most of the solar energy, so high absorption efficiency in the visible band must be ensured. Planar structures with similar dimensions achieved only about 80% absorption when the wavelength of incident light was close to 500 nm. Comparison of the absorption curves for the original model and the planar structure showed that the presence of an artificially designed cross-shaped

Preprints (www.preprints.org) | NOT PEER-REVIEWED | Posted: 5 July 2022 doi:10.20944/preprints202207.0060.v1

resonator and a triangular array had a significant impact on the absorption bandwidth and peak. This was also supported by previous experimental results: absorbers with special shapes (e.g., disc) are more efficient than absorbers with stacked structures[22, 28].

Fig. 2(d) shows that the use of different materials caused the whole absorption curve to go up and down at different wavelengths of incident light. The entire curve also underwent redshift or blueshift, depending on the materials. It is evident that although W, Ti, Ni, and Cr all have a high imaginary refractive index, using tungsten and titanium for the top array and substrate, respectively, optimized the structure's absorption. This was because the cross-shaped resonator, triangular array, and substrate led to incomplete overlap of the absorption bands. Using only one metal material resulted in a narrower overall absorption bandwidth and a lower overall average absorption rate. Choosing different materials caused the entire absorption peak to appear in different regions, so selecting other materials for the top array as well as the substrate maximized the absorption and yielded the widest bandwidth.

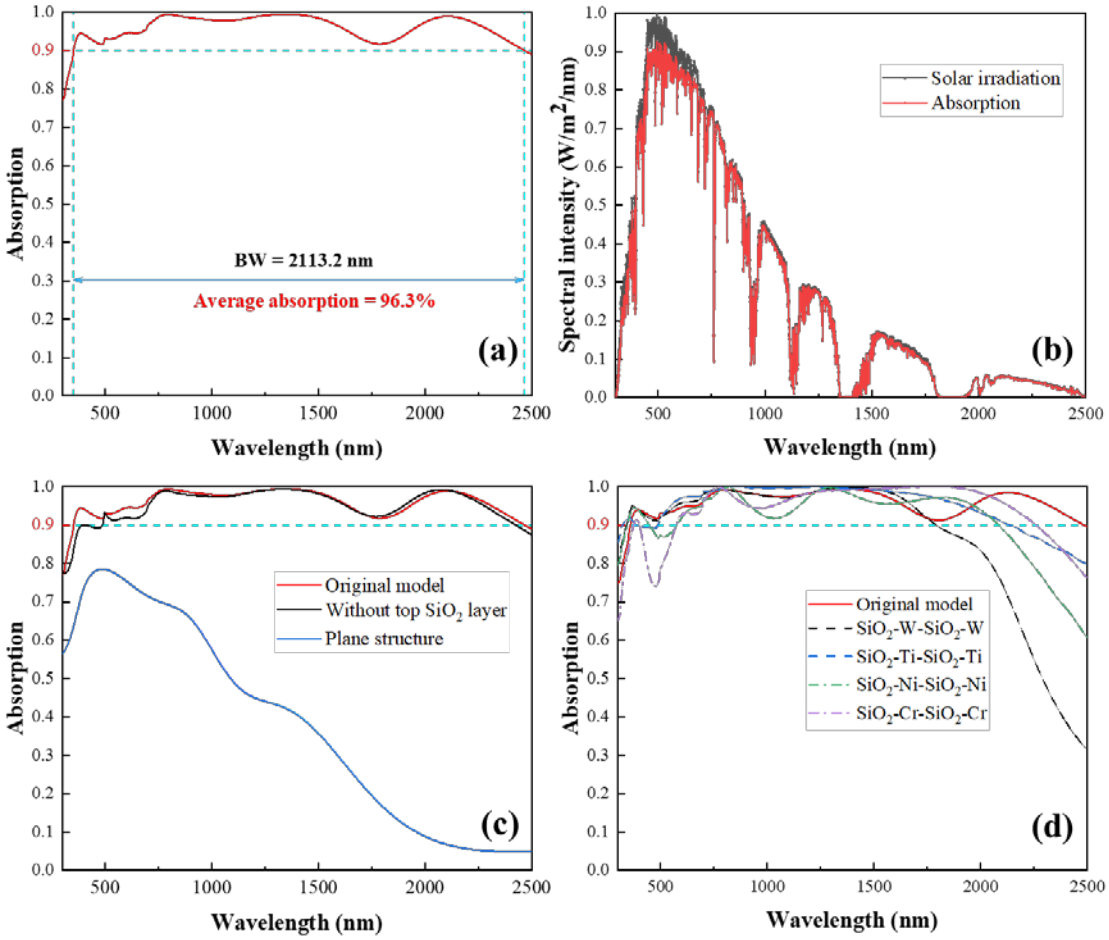

Fig. 2. (a) Absorption curve of the original model. (b) Solar spectral intensity and absorption curve. (c) Absorption of original model, model without top SiO_2 layer, and planar structure. (d) Absorption of original model and models using other metal materials.

To explain why this absorbing structure has broadband and efficient absorption, we scanned the electric and magnetic fields when the incident light was vertically incident on this structure without polarization at specific wavelengths; the results are presented in Figs. 3(a)-(i). Among these, we selected the specific wavelengths 800, 1320, and 2120 nm, corresponding to the three peaks in the absorption curve. By scanning the electric field in the X-Y plane in Figs. 3(a)-(c), we found that as the incident light wavelength increased, the electric field intensity at the boundary of the triangular array decreased and the electric field intensity at the edge of the cross-shaped resonator increased. This was because the electric field was generated by localized surface plasmon resonance (LSPR) under subwavelength conditions. The dimensions of the cross-shaped resonator were slightly larger than those of the triangular array, and both were smaller than the incident light wavelength. Therefore, as the incident light wavelength increased, the LSPR gradually increased around the central cross-shaped resonator and gradually decreased around the triangular array. By scanning the electric field in the X-Z plane in Figs. 3(d)-(f), we found that a strong electric field was also excited in the SiO_2 dielectric layer below the cross-shaped resonator; this was the result of the joint action of the propagating surface plasmon resonance (PSPR) and the FP cavity.

 doi:10.20944/preprints202207.0060.v1

By observing the magnetic field distribution in the X-Z plane in Figs. 3(g)-(i), we also assessed the combination of PSPR, LSPR, and the FP cavity. The magnetic field in the SiO_2 dielectric layer was generated from cooperation between the PSPR and the FP cavity. Since the cross-shaped resonator and the triangular array were covered by lossless dielectric layers, a strong PSPR was generated. In our design, adding lossless dielectric layers above and below the cross-shaped resonator and the triangular array effectively provided high-quality SPRs[29]. Moreover, our chosen material (tungsten) has a large imaginary refractive index and possesses strong intrinsic metal loss. Therefore, the dimensions of our design allowed the cross-shaped resonator and triangular array to provide good absorption in a large wavelength range of incident light.

Fig. 3. (a)-(c): Electric field scanning in the X-Y plane. (d)-(f): Electric field scanning in the X-Z plane. (g)-(i): Magnetic field scanning in the X-Z plane.

In Figure 4, we explore what the cross-shaped resonator and the triangular array contributed to the absorption for the same parameters. In the incident light wavelength range of 300–500 nm, the absorption curves of the original model, the structure without

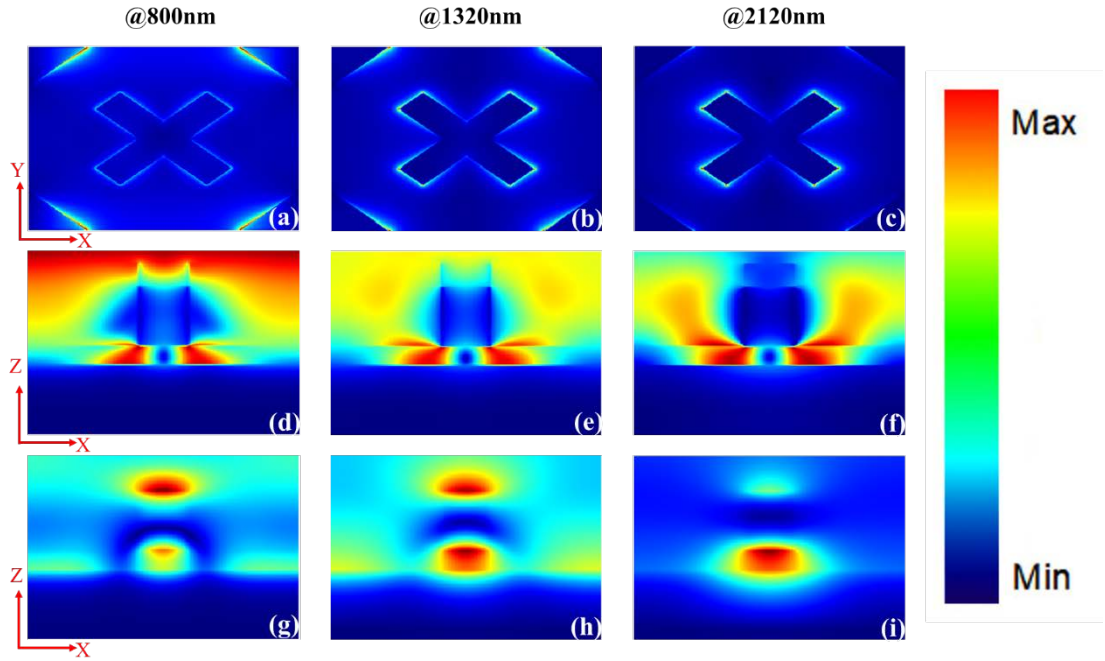

a cross-shaped resonator, and the structure without a triangular array had similar shapes, and the average absorption of the original model was the highest. The three absorption curves peaked successively at an incident wavelength of about 800 nm. We think the combined effect of the triangular array and the cross-shaped resonator located the absorption peak of the complete structure in the middle of the two, and the absorption of the complete structure was provided by the cross-shaped resonator and the triangular array together. At an incident light wavelength of about 2000 nm, the absorption curve of the structure without a triangular array peaked, while the absorption curve of the structure without a cross-shaped resonator slowly decreased. The combined effect of the two resulted in an absorption peak when the wavelength of incident light was 2100 nm. Although this absorption peak was slightly lower than the peak produced by the structure without the triangular array, it was broad, resulting in a bandwidth of perfect absorption greater than 2000 nm. We conclude that combining a cross-shaped resonator and a triangular array can facilitate the effect of plasmon resonance and the FP cavity, resulting in better absorption of sunlight.

 doi:10.20944/preprints202207.0060.v1

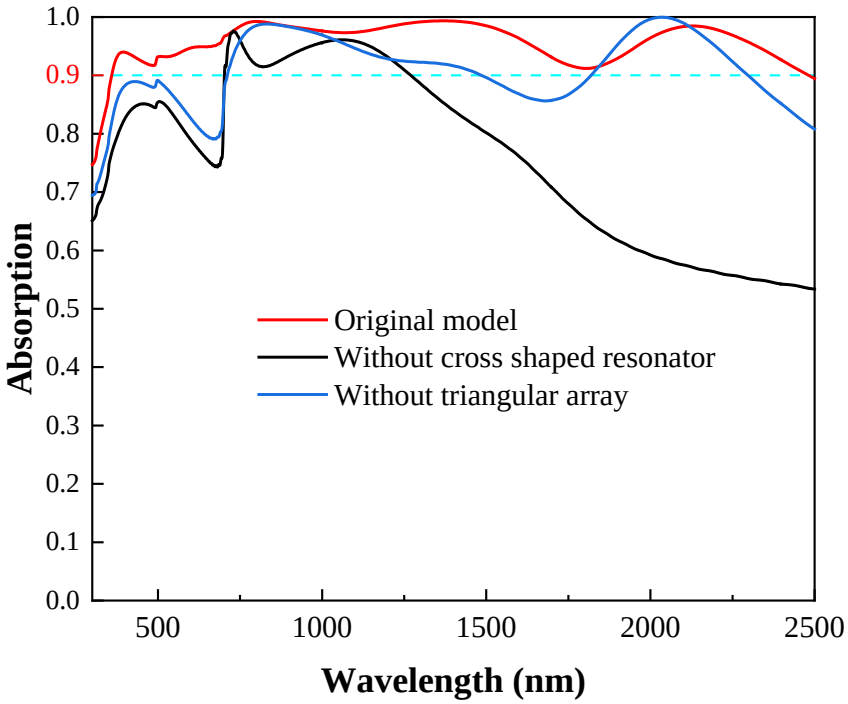

Fig. 4. Comparison of the absorption curves of the structure without a cross-shaped resonator, the structure without a triangular array, and the original model.

After analyzing the reasons for the structure's good absorption, we know that the sizes of the cross-shaped resonator and triangular array are closely related to its performance. To obtain the best microwave absorption performance, we performed a series of sweeps of the cross-shaped resonator and triangular array.

Figure 5(a) shows the absorption performance of the resonator for different length and width conditions. As the resonator's size increased, there was a significant redshift of the absorption peak: when the length (l) and width (w) increased from 350 and 50 nm to 470 and 130 nm, respectively, the wavelength value at the absorption peak increased from approximately 1850 to 2500 nm. Conversely, as the size decreased, the absorption was higher when the wavelength of the incident light was smaller. Since energy scattered by the sun is mainly concentrated in sunlight, whose wavelength ranges from 300 to 2500 nm, to achieve both high and broadband absorption, we chose a compromise size: l = 410 nm and w = 90 nm. When we observed the effects on absorption caused by changing the triangular array parameters (Fig. 5(b)), similar results were seen: the position of the absorption peak gradually redshifted when the side length (t) increased from 110 to 190 nm. We chose t = 150 nm as the final parameter for working with the cross-shaped resonator to achieve the best solar absorption performance.

Figure 5(c) shows that as the height of the cross-shaped resonator and triangular array increased, the width of the two absorption peaks gradually increased, but when the height of the tungsten layer increased to a certain level, the width of the absorption peak gradually stopped expanding, and the peak of the absorption peak decreased slightly. To achieve the best absorption effect, we chose 200 nm as the height of both, which yielded an absorption bandwidth above 2000 nm and good absorption in the visible and UV regions (300–760 nm).

Preprints (www.preprints.org) | NOT PEER-REVIEWED | Posted: 5 July 2022 doi:10.20944/preprints202207.0060.v1

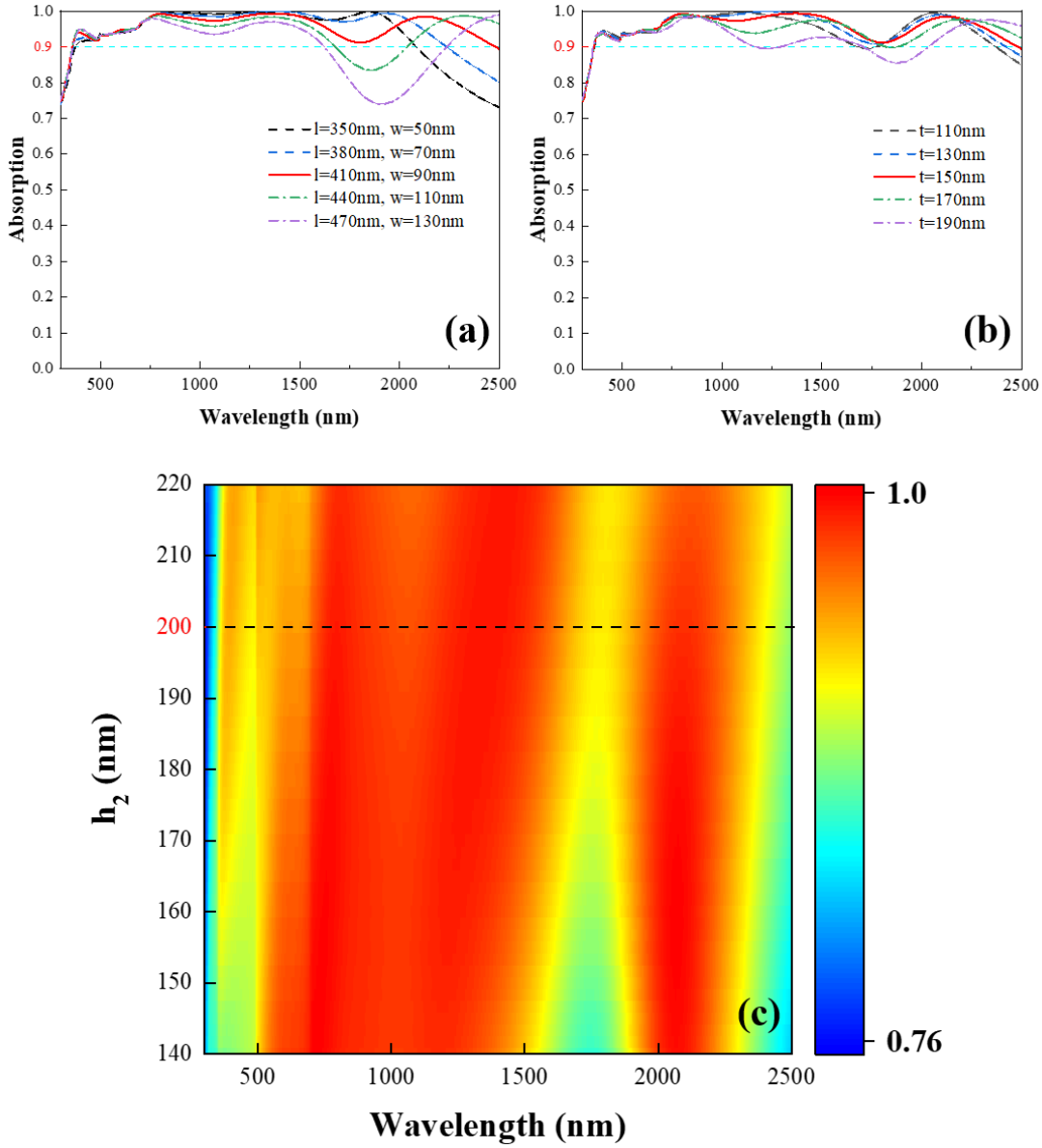

Fig. 5. (a) Absorption of cross-shaped resonator with different lengths (l) and widths (w). (b) Absorption of triangular array with different side lengths (t). (c) Cross-shaped resonator and triangular array height scan (h_2).

To explore which material (magnesium fluoride (MgF_2), SiO_2, alumina (Al_2O_3), silicon nitride (Si_3N_4), or TiO_2) was the most suitable lossless dielectric for this structure, we compared their absorption properties, as shown in Fig. 6(a). The materials' refractive indices were taken from the *Handbook of Optical Constants of Solids*[27]. We found that SiO_2, a very common material, gave the best solar absorption performance for the whole structure. We therefore chose to use it as the lossless dielectric material for this structure.

Based on previous electric and magnetic field scans, we knew that to have good solar absorption performance, we needed to excite the strongest plasmon resonance from the lossless dielectric layer under the cross-shaped resonator and the triangular array. A proper dielectric thickness (h_3) delicately combined the joint action of the FP cavity and PSPR to achieve the most effective absorption. We swept the height of h_3 and highlighted the regions where the absorption was above 90%: in Figure 6(b), the more the absorption exceeds 90%, the closer the color is to red, while the regions where the absorption is below 90% are uniformly blue to highlight the parameters that optimized the absorption. As h_3 increased, the width of the high absorption region first gradually increased and then decreased. We knew there were two wide absorption regions and a narrow absorption peak. As the thickness of the lossless dielectric layer increased, the two broad absorption regions tended to gradually approach each other, and then gradually

Preprints (www.preprints.org) | NOT PEER-REVIEWED | Posted: 5 July 2022 doi:10.20944/preprints202207.0060.v1

moved away after the closest distance. As the radiation intensity in the incident light wavelength range of 300–500 nm is relatively high, we chose h_3 = 60 nm as the thickness of the dielectric layer to achieve perfect absorption.

Fig. 6. (a) Absorption of different dielectric materials: polyethylene, silica, quartz, vanadium dioxide, and alumina. (b) Thickness sweep of lossless dielectric layer.

To theoretically assess why our proposed structure has good solar absorption performance, we analyzed the structure using effective medium theory and the impedance-matching principle, and used the following formula to calculate the structure's

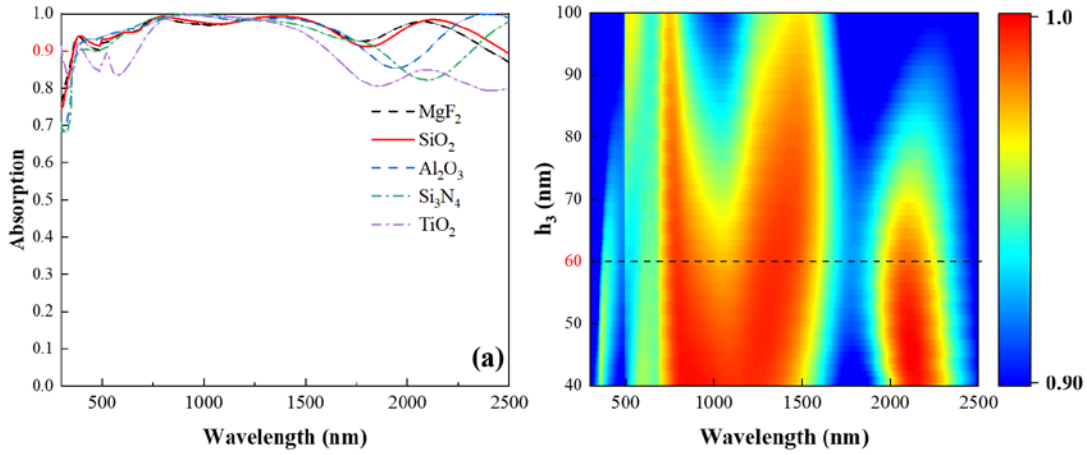

impedance[30, 31]:

$$Z = \pm\sqrt{\frac{(1+S_{11})^2 - S_{21}^{\ 2}}{(1-S_{11})^2 - S_{21}^{\ 2}}} \tag{2}$$

$$S_{11} = S_{22} = \frac{i}{2}\left(\frac{1}{Z} - Z\right)\sin(nkd) \tag{3}$$

$$S_{21} = S_{12} = \frac{1}{\cos(nkd) - \frac{i}{2}\left(Z + \frac{1}{2}\right)\sin(nkd)} \tag{4}$$

In these formulas, S_{11}, S_{22}, S_{21}, and S_{12} are all S parameters, where $S_{11} = R$ and $S_{12} = T = 0$. In addition, n is the reflection index, k is the wave vector, and d is the thickness of the designed structure. In free space, when the plane wave is transmitted to the surface of the medium, the medium's reflectivity is:

$$R = \frac{Z_0 - Z_{in}}{Z_0 + Z_{in}} \tag{5}$$

where Z_0 is the impedance of the free space and Z_{in} is the impedance of the incident material in contact with the free space. In general, the real part of the impedance in free space is 1 and the imaginary part is 0. According to the impedance-matching principle, when the impedance of the material is close to that of the free space, the reflection coefficient is very small. Since T and R are very small and $A = 1 - R - T$, when A is close to 1, excellent absorption performance can be obtained for the whole structure. In Fig. 7, we can see that in the region from visible to near infrared, the real part of the structure's impedance is close to 1 and the imaginary part is close to 0. Therefore, we believe this structure has good absorption efficiency in free space.

Preprints (www.preprints.org) | NOT PEER-REVIEWED | Posted: 5 July 2022 doi:10.20944/preprints202207.0060.v1

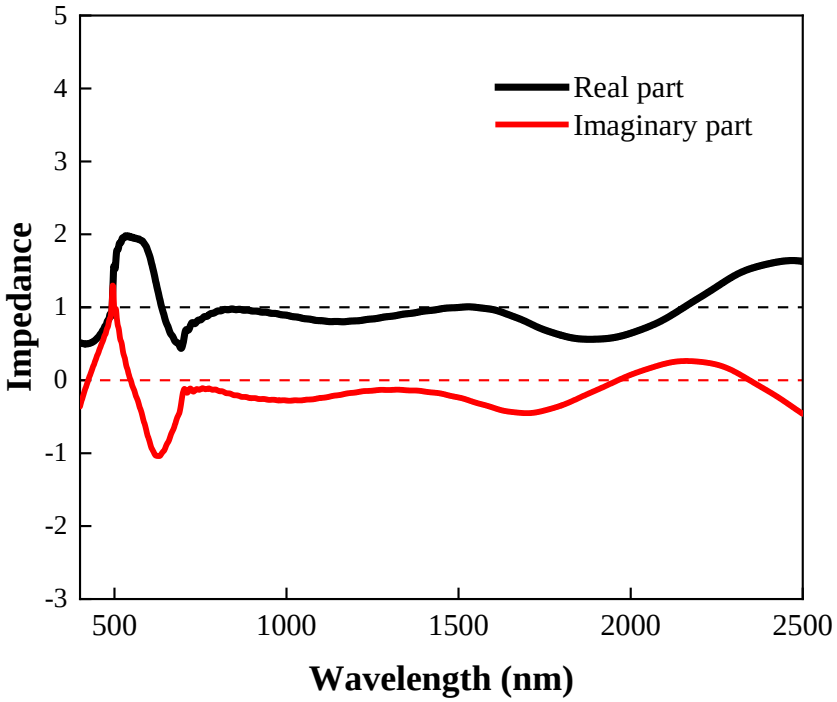

Fig. 7 The impedance of the proposed structure.

When this absorber is actually put into use, the light will not always be vertically incident without polarization. We therefore scanned the structure at different polarization angles and different incident angles. The results in Fig. 8(a) show there was little change in the structure's absorption with increasing polarization angle during the change from TE to TM polarization (0° to 90°). This was because our proposed structure is not only axisymmetric but also centrosymmetric. The high degree of symmetry kept the overall absorption stable under different conditions of polarized light incidence. Moreover, the absorber maintained perfect absorption in the incident light wavelength range of 700–2050 nm, and high absorption (>80%) in the incident light wavelength range of 300–2350 nm, with different and increasing incidence angles. We thus believe this structure would be able to absorb solar energy efficiently in practical application scenarios.

Fig. 8. (a) Absorptivity at different incident angles. (b) Absorptivity at different polarization angles.

4. Conclusions

In this paper, we have proposed a solar absorber based on the FDTD method that can absorb solar energy across the visible and

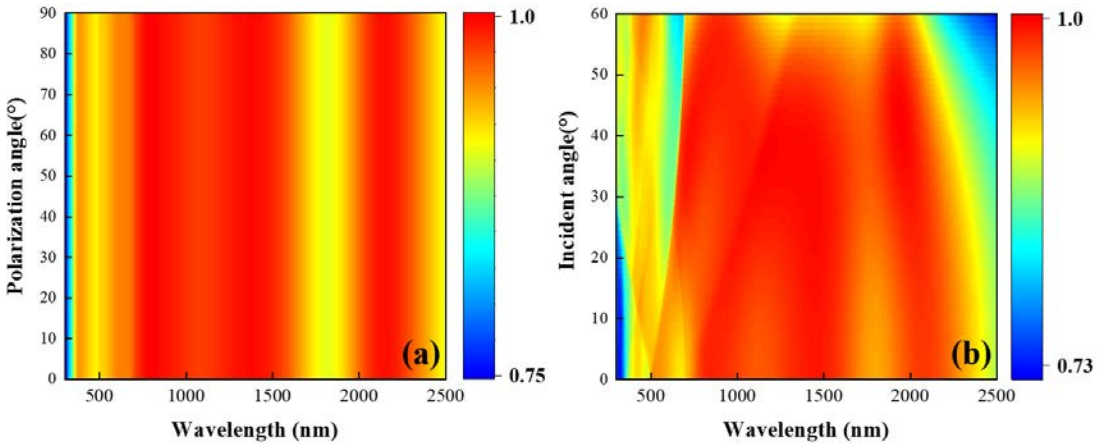

near-infrared regions. The width of the perfect absorption band reaches 2113.2 nm, within which the average absorption is 96.3% and the maximum is 99.4%. Through theoretical analysis and electromagnetic field scanning, we explained why the structure is able to achieve broadband absorption and compared the effect of different materials and dimensions on the overall absorption. Finally, sweep diagrams of the polarization angle and incident angle showed that the structure is independent of the polarization angle and

insensitive to the incident angle, allowing it to be used in practical application scenarios. With the increasing demand for renewable energy, this absorber could play a major role in solar energy absorption, thermoelectric conversion, and many other applications.

Funding

This work was supported by Fujian Provincial Natural Science Foundation 2020J01712; the Second Youth Talent Support Program of Fujian Province (Eyas Plan of Fujian Province 2021); the Fujian Provincial Department of Science and Technology 2019H0022; Science Fund for Distinguished Young Scholars of Fujian Province 2020J06025; Youth Talent Support Program of Jimei University ZR2019002; Innovation Fund for Young Scientists of Xiamen under Grant 3502Z20206021; Xiamen Marine and Fishery Development Special Fund 20CZB014HJ03;

Disclosures

The authors declare that there are no conflicts of interest related to this article.

Data availability

No data were generated or analyzed in the present research.

References

1. Gielen, D., et al., *The role of renewable energy in the global energy transformation.* Energy Strategy Reviews, 2019. **24**: p. 38-50.
2. Chueh, C.-C., et al., *Harnessing MOF materials in photovoltaic devices: recent advances, challenges, and perspectives.* Journal of Materials Chemistry A, 2019. **7**(29): p. 17079-17095.
3. Kumar, L., M. Hasanuzzaman, and N.A. Rahim, *Global advancement of solar thermal energy technologies for industrial process heat and its future prospects: A review.* Energy Conversion and Management, 2019. **195**: p. 885-908.
4. Mofijur, M., et al., *Phase Change Materials (PCM) for Solar Energy Usages and Storage: An Overview.* Energies, 2019. **12**(16).
5. Wilson, G.M., et al., *The 2020 photovoltaic technologies roadmap.* Journal of Physics D-Applied Physics, 2020. **53**(49).
6. Yin, L., et al., *MXenes for Solar Cells.* Nano-Micro Letters, 2021. **13**(1).
7. Kang, Q., et al., *Tunable Thermal Camouflage Based on GST Plasmonic Metamaterial.* Nanomaterials, 2021. **11**(2).
8. Liu, X., et al., *Taming the Blackbody with Infrared Metamaterials as Selective Thermal Emitters.* Physical Review Letters, 2011. **107**(4).
9. Bai, Q., *Manifestation of the spontaneous parity-time symmetry breaking phase transition in hot-electron photodetection based on a tri-layered metamaterial.* Nanophotonics, 2019. **8**(3): p. 495-504.
10. Bai, Q., *Phase-coupled simultaneous coherent perfect absorption and controllable hot-electron photodetection in Schottky junction metamaterial.* Nanophotonics, 2020. **9**(1): p. 211-224.
11. Kong, J., et al., *Hot electron plasmon-protected solar cell.* Optics Express, 2015. **23**(19): p. A1087-A1095.
12. Sakhdari, M., et al., *Efficient, broadband and wide-angle hot-electron transduction using metal-semiconductor hyperbolic metamaterials.* Nano Energy, 2016. **26**: p. 371-381.
13. Agarwal, S. and Y.K. Prajapati, *Metamaterial based sucrose detection sensor using transmission spectroscopy.* Optik, 2020. **205**.
14. Chen, Y.S., et al., *Fingerprint detection in the mid-infrared region based on guided-mode resonance and phonon-polariton coupling of analyte.* Optics Express, 2021. **29**(23): p. 37234-37244.
15. Hoque, A. and M.T. Islam, *Numerical Analysis of Single Negative Broadband Metamaterial Absorber Based on Tri Thin Layer Material in Visible Spectrum for Solar Cell Energy Harvesting.* Plasmonics, 2020. **15**(4): p. 1061-1069.
16. Lin, K.T., et al., *Structured graphene metamaterial selective absorbers for high efficiency and omnidirectional solar thermal energy conversion.* Nature Communications, 2020. **11**(1).
17. Li, J.K., et al., *Tunable Broadband Solar Energy Absorber Based on Monolayer Transition Metal Dichalcogenides Materials Using Au Nanocubes.* Nanomaterials, 2020. **10**(2).
18. Qin, F., et al., *A Tunable Triple-Band Near-Infrared Metamaterial Absorber Based on Au Nano-Cuboids Array.* Nanomaterials, 2020. **10**(2).
19. Elrashidi, A. and M.M. Tharwat, *Broadband absorber using ultra-thin plasmonic metamaterials nanostructure in the visible and near-infrared regions.* Optical and Quantum Electronics, 2021. **53**(8).
20. Liu, Z., et al., *Ultra-broadband perfect solar absorber by an ultra-thin refractory titanium nitride meta-surface.* Solar Energy Materials and Solar Cells, 2018. **179**: p. 346-352.
21. Yu, P.Q., et al., *A numerical research of wideband solar absorber based on refractory metal from visible to near infrared.* Optical Materials, 2019. **97**.
22. Liu, J., et al., *Ultra-Broadband Infrared Absorbers Using Iron Thin Layers.* Ieee Access, 2020. **8**: p. 43407-43412.
23. Wu, P.H., et al., *Ultra-Wideband and Wide-Angle Perfect Solar Energy Absorber Based on Titanium and Silicon Dioxide Colloidal Nanoarray Structure.* Nanomaterials, 2021. **11**(8).
24. Qin, F., et al., *Ultra-broadband and wide-angle perfect solar absorber based on TiN nanodisk and Ti thin film structure.* Solar Energy Materials and Solar Cells, 2020. **211**.
25. Roostaei, N., et al., *Plasmonic wideband and tunable absorber based on semi etalon nano structure in the visible region.* Physica Scripta, 2021. **96**(3).
26. Matthew, J.A.D., *CRC HANDBOOK OF CHEMISTRY AND PHYSICS - WEAST,RC.* Nature, 1988. **331**(6152): p. 127-127.

27. Palik, E.D., *Preface*, in *Handbook of Optical Constants of Solids*, E.D. Palik, Editor. 1985, Academic Press: Boston. p. xvii-xviii.
28. Liu, J., et al., *Wide-Angle Polarization-Independent Ultra-Broadband Absorber from Visible to Infrared.* Nanomaterials, 2020. **10**(1).
29. Wang, B., et al., *High-Q Plasmonic Resonances: Fundamentals and Applications.* Advanced Optical Materials, 2021. **9**(7).
30. Smith, D.R., et al., *Electromagnetic parameter retrieval from inhomogeneous metamaterials.* Physical Review E, 2005. **71**(3).
31. Szabo, Z., et al., *A Unique Extraction of Metamaterial Parameters Based on Kramers-Kronig Relationship.* Ieee Transactions on Microwave Theory and Techniques, 2010. **58**(10): p. 2646-2653.